The combustion products species concentrations were measured in the exhaust gas stream using a Multigas 2030 spectrometer analyzer (MKS Instruments).

The MKS 2030 spectrometer works based on Fourier Transform Infrared (FTIR) principle and can acquire multiple gas species at same time. The detection limit is 1 ppm for CO and 0.5 ppm for formaldehyde, NO, NO_2, and ethanol; the equipment accuracy is 5% for all the chemical species. Emission data were adjusted for dry basis and corrected to 3% oxygen for a pattern of oxygen consumption in the relation of the oxygen presented in pure air (considered here 20.9%).

RESULTS

To study the behavior and operating conditions of the internal combustion engine, images were acquired through the bottom view of the combustion chamber. This visualization allows a better analysis and in obtaining information about flame propagation. Figures 4-6 show the flame propagation images for combustion at the speed of 1500 rpm, for λ 1.0, 1.2 and 1.4, respectively, from spark ignition.

From this, it is observed that variability and a decentralization of the flame is provided as the increase in air dilution occurs. In addition to a lower definition of the flame edge, greater variability of its circularity, a lower propagation speed is observed with the increase of air dilution. Some of the possible reasons for the displacement of the flame with the increase in dilution could be the more intense tumble movement characteristic of this engine and the greater amount of fuel in the region of the intake valve (Abrantes, 2017).

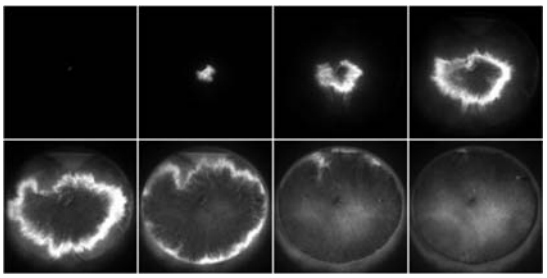

Figure 3. The sequence of images from the bottom view of the flame propagation from spark ignition for 1500 rpm and air-fuel ratio λ = 1.0.

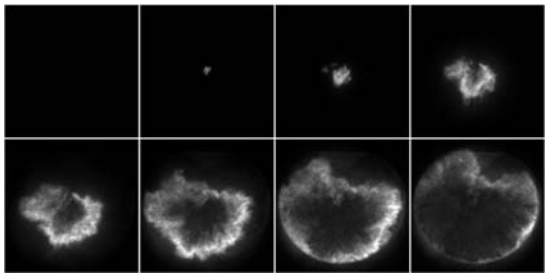

Figure 4. The sequence of images from the bottom view of the flame propagation from spark ignition for 1500 rpm and air-fuel ratio λ = 1.2.

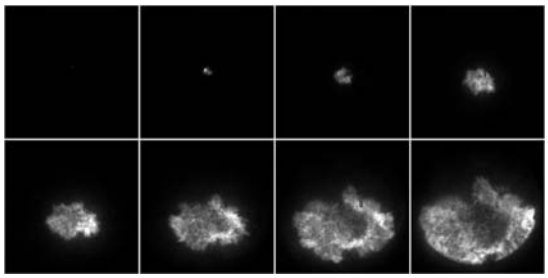

Figure 5. The sequence of images from the bottom view of the flame propagation from spark ignition for 1500 rpm and air-fuel ratio λ = 1.4.

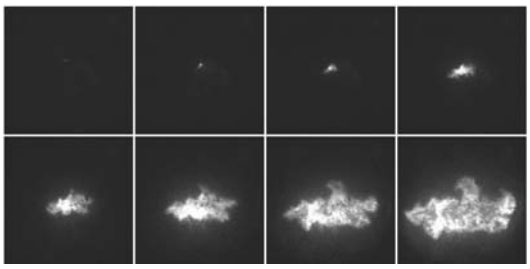

Figure 6. The sequence of images from the bottom view of the flame propagation from spark ignition for 1500 rpm and air-fuel ratio λ = 1.4.

Table 1 to Table 4 show the IMEP, maximum cylinder pressure, AI50% and lambda values for a burn condition for an average of the last 100 engine cycles in operation for the 1500 rpm experiments and lambda values of 1.0, 1.2, 1.4 and 1.5.

In these figures, it is possible to observe that the IMEP coefficient of variability (COV) is proportional to the increase in the lambda value, with a higher value of COVImep = 16.32% for a lambda of 1.5 (Table 4). It is also possible to notice that the average behavior of the IMEP presents several instabilities during the 100 measured cycles.

Table 1. Experimental results for the test at 1500 rpm and lambda 1.0. Top image: lambda and IMEP behavior during the last 100 cycles; bottom image:

summary of the average indicating results of the last 100 cycles.

	IMEP [bar]	PMAX [bar]	AI10% [deg]	AI50% [deg]	Lambda -
Min	2.98	15.81	1.00	9.00	1.01
Mean	3.04	17.50	3.05	12.61	1.03
Max	3.16	19.20	4.75	16.50	1.05
Std	0.040	0.738	0.958	1.60	0.009
Cov%	1.30	4.22	31.42	12.67	0.833

Speed [rpm]	P Intake [mbar]	Throttle %	IGN [ºCA]
1500	-417	7.6	-14
SOI [ºCA]	DOI [ms]	mAir [kg/h]	P Rail [bar]
-290	3.32	10.65	100

Table 2. Experimental results for the test at 1500 rpm and lambda 1.2. Top image: lambda and IMEP behavior during the last 100 cycles; bottom image: summary of the average indicating results of the last 100 cycles.

	IMEP [bar]	PMAX [bar]	AI10% [deg]	AI50% [deg]	Lambda -
Min	2.95	13.39	3.00	11.75	1.20
Mean	3.05	16.15	5.60	16.23	1.23
Max	3.16	18.25	10.25	23.00	1.27
Std	0.038	1.06	1.57	2.38	0.013
Cov%	1.25	6.54	28.12	14.67	1.03

Speed [rpm]	P Intake [mbar]	Throttle %	IGN [ºCA]
1500	-366	8.2	-14
SOI [ºCA]	DOI [ms]	mAir [kg/h]	P Rail [bar]
-290	3.15	11.73	100

Table 3. Experimental results for the test at 1500 rpm and lambda 1.4. Top image: lambda and IMEP behavior during the last 100 cycles; bottom image: summary of the average indicating results of the last 100 cycles.

	IMEP [bar]	PMAX [bar]	AI10% [deg]	AI50% [deg]	Lambda -
Min	2.57	10.37	7.00	20.00	1.40
Mean	3.00	12.85	10.86	26.61	1.43
Max	3.23	15.50	16.25	36.50	1.47
Std	0.145	1.28	2.15	4.12	0.016
Cov%	4.83	9.97	19.80	15.48	1.14

Speed [rpm]	P Intake [mbar]	Throttle %	IGN [ºCA]
1500	-301	9.2	-14
SOI [ºCA]	DOI [ms]	mAir [kg/h]	P Rail [bar]
-290	3.14	13.27	100

Table 4. Experimental results for the test at 1500 rpm and lambda 1.5. Top image: lambda and IMEP behavior during the last 100 cycles; bottom image: summary of the average indicating results of the last 100 cycles.

	IMEP [bar]	PMAX [bar]	AI10% [deg]	AI50% [deg]	Lambda -
Min	1.15	10.36	10.00	24.75	1.47
Mean	2.24	10.72	16.29	37.69	1.52
Max	2.81	13.35	25.00	50.00	1.58
Std	0.365	0.537	3.12	6.07	0.027
Cov%	16.32	5.00	19.13	16.10	1.77

Speed [rpm]	P Intake [mbar]	Throttle %	IGN [ºCA]
1500	-296	9.4	-14
SOI [ºCA]	DOI [ms]	mAir [kg/h]	P Rail [bar]
-290	3.09	13.7	100

Figure 7 shows the average cylinder pressure curves for all cases of 1500 rpm. It is possible to see the influence of increased air and the influence of variability on the IMEP for cases with 1.4 and 1.5 lambda. In addition, it is seen that the dilution causes the pressure curve displacement, which can also be observed in the values of AI10% and AI50% of the previous tables and in the burnt mass fraction graphs where the flame propagation is slower when measured that dilution occurs. This behavior is also due to the fixed ignition advance.

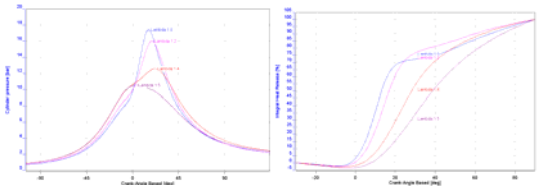

Figure 7. Average cylinder pressure curves and average integral heat release curves for 1500 rpm; IMEP 3.0 bar, for the bottom view experiments.

From Fig. 8 to Fig. 10, the average results of gas emissions for the experiments performed with 1500 rpm and IMEP 3.0 are presented.

It was observed that carbon dioxide (CO_2) presented a slight decrease with increasing dilution in air, however, its value remained close. As for carbon monoxide (CO) and NO_X emissions, a large decrease was provided as dilution by air occurred. There is a significant decrease for NO_X (about 10 times less between $\lambda = 1$ and $\lambda = 1.43$). With the increase in the amount of air present in the combustion chamber, the decrease in temperature caused by this leads to less formation of thermal NOx, due to the lower burning temperature.

It is also observed that formaldehyde and THC-ethanol emissions increased slightly from $\lambda = 1$ to $\lambda = 1.25$ and decreased between $\lambda = 1.25$ and $\lambda = 1.43$. Emissions from unburned ethanol have been steadily increasing with increasing dilution.

In lean combustion, excess air can act in addition to reducing the flame temperature, but also limiting the ability of the reactions to reach equilibrium, which can lead to an increase in exhaust hydrocarbons. Furthermore, cooling the combustion chamber wall can contribute to cooling (Dunn-Rankin et. al., 2016 and Turns, 2013).

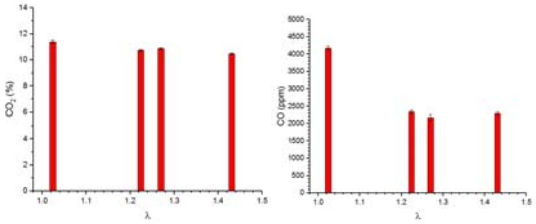

Figure 8. Emissions gas measurement of CO_2 and CO, 1500 rpm, IMEP 3.0 bar.

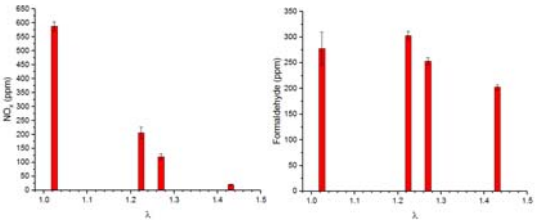

Figure 9. Emissions gas measurement of NOx and formaldehyde, 1500 rpm, IMEP 3.0 bar.

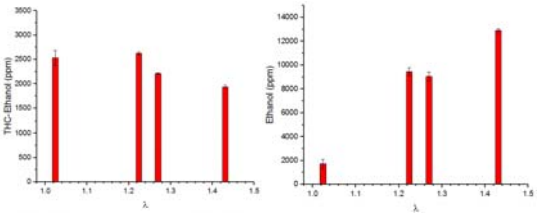

Figure 10. Emissions gas measurement of THC-ethanol and unburned ethanol, 1500 rpm, IMEP 3.0 bar.

Similar to the 1500 rpm data, the images were also acquired from the bottom view, obtaining the combustion flame propagation for the same air-fuel ratios for 2500 rpm in Fig. 11 to Fig. 13.

With the same behavior as the 1500 rpm images, the 2500 rpm images show an increase in the variability, distortion and displacement of the flame with the increase in air dilution. Furthermore, the lowest propagation speed is also observed.

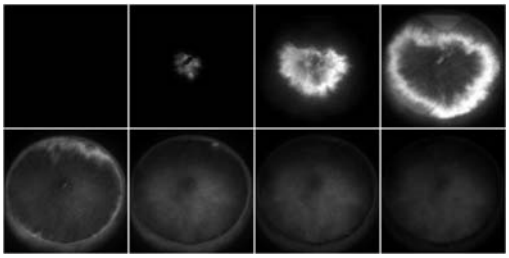

Figure 11. The sequence of images from the bottom view of the flame propagation from spark ignition for 2500 rpm and air-fuel ratio λ = 1.0.

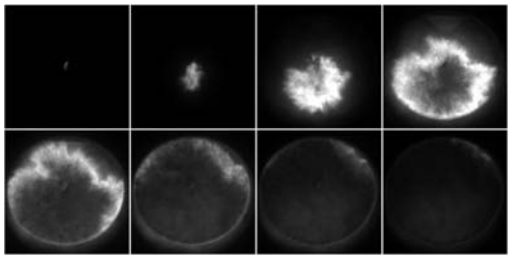

Figure 12. The sequence of images from the bottom view of the flame propagation from spark ignition for 2500 rpm and air-fuel ratio λ = 1.2.

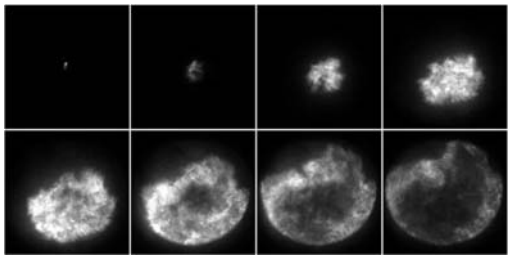

Figure 13. The sequence of images from the bottom view of the flame propagation from spark ignition for 2500 rpm and air-fuel ratio λ = 1.4.

Table 5 to Table 8 show IMEP, maximum cylinder pressure, AI50% and lambda values for an ignition condition for an average of the last 100 engine cycles in drive operation for the experiments at 2500 rpm and lambda values of 1.0, 1.2, 1.3 and 1.4, respectively.

In these figures, it is possible to observe that the conditions are similar to the 1500 rpm experiments. It was observed that the IMEP coefficient of variability (COV) is proportional to the increase in the lambda value, with a higher value of COV = 27.74% for a lambda of 1.4 (Tab. 8), it is also possible to notice that the average behavior of the IMEP presents several instabilities during the 100 measured cycles.

Table 5. Experimental results for the test at 2500 rpm and lambda 1.0. Top image: lambda and IMEP behavior during the last 100 cycles; bottom image: summary of the average indicating results of the last 100 cycles.

	IMEP [bar]	PMAX [bar]	AI10% [deg]	AI50% [deg]	Lambda -
Min	1.69	11.62	-3.50	4.00	0.993
Mean	1.79	13.08	-0.860	8.00	1.00
Max	1.87	14.23	2.00	12.50	1.01
Std	0.037	0.597	1.26	1.97	0.005
Cov%	2.06	4.56	146.5	24.67	0.464

Speed [rpm]	P Intake [mbar]	Throttle %	IGN [ºCA]

1500	-548	7.6	-20
SOI [ºCA]	DOI [ms]	mAir [kg/h]	P Rail [bar]
-290	2.15	11.21	100

Table 6. Experimental results for the test at 2500 rpm and lambda 1.2. Top image: lambda and IMEP behavior during the last 100 cycles; bottom image: summary of the average indicating results of the last 100 cycles.

	IMEP [bar]	PMAX [bar]	AI10% [deg]	AI50% [deg]	Lambda -
Min	1.69	9.98	-1.00	7.00	1.20
Mean	1.80	11.60	2.40	13.56	1.21
Max	1.89	13.63	6.25	19.50	1.22
Std	0.045	0.823	1.62	2.87	0.005
Cov%	2.48	7.09	67.72	21.15	0.426

Speed [rpm]	P Intake [mbar]	Throttle %	IGN [ºCA]
1500	-516	8.2	-20
SOI [ºCA]	DOI [ms]	mAir [kg/h]	P Rail [bar]
-290	1.97	12.48	100

Table 7. Experimental results for the test at 2500 rpm and lambda 1.3. Top image: lambda and IMEP behavior during the last 100 cycles; bottom image: summary of the average indicating results of the last 100 cycles.

	IMEP [bar]	PMAX [bar]	AI10% [deg]	AI50% [deg]	Lambda -
Min	1.66	8.18	10.00	12.50	1.30
Mean	1.83	10.49	5.22	18.75	1.32
Max	1.91	12.34	12.00	27.50	1.35
Std	0.058	1.00	2.39	3.74	0.009
Cov%	3.15	9.58	45.80	19.94	0.707

Speed [rpm]	P Intake [mbar]	Throttle %	IGN [ºCA]
1500	-489	8.5	-20
SOI [ºCA]	DOI [ms]	mAir [kg/h]	P Rail [bar]
-290	2.03	13.68	100

Table 8. Experimental results for the test at 2500 rpm and lambda 1.4. Top image: lambda and IMEP behavior during the last 100 cycles; bottom image: summary of the average indicating results of the last 100 cycles.

	IMEP [bar]	PMAX [bar]	AI10% [deg]	AI50% [deg]	Lambda -
Min	-0.613	7.14	4.00	16.00	1.40
Mean	1.32	8.10	11.50	30.52	1.44
Max	1.90	10.82	40.00	56.00	1.58
Std	0.366	0.872	5.60	7.26	0.028
Cov%	27.74	10.76	48.67	23.80	1.96

Speed [rpm]	P Intake [mbar]	Throttle %	IGN [ºCA]
1500	-477	9	-20
SOI [ºCA]	DOI [ms]	mAir [kg/h]	P Rail [bar]
-290	1.94	13.96	100

Figure 14 shows the curves of the average cylinder pressure for all cases of 2500 rpm. It is possible to see the influence of the increase in air and the influence of variability on the IMEP for the case with lambda 1.4. In addition, the influence of air dilution on the burned mass fraction during the combustion process is observed, showing that the flame propagation is slower for lean mixtures, a condition similar to the 1500 rpm cases.

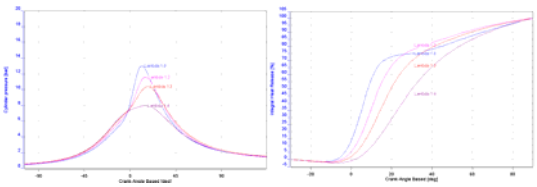

Figure 14. Average cylinder pressure curves and average integral heat release curves for 2500 rpm; IMEP 1.8 bar cases, for the bottom view experiments.

From Fig. 15 to Fig. 17, the average results of gas emissions for the experiments performed with 2500 rpm are presented. For carbon dioxide (CO_2) emissions, a slight increase was shown between $\lambda = 1$ and $\lambda = 1.21$ and a slight decrease between $\lambda = 1.24$ and $\lambda = 1.34$. However, the results are close. As for the NO_X emission, there is a decrease with dilution (about 7 times less between $\lambda = 1$ and $\lambda = 1.34$). For formaldehyde and THC-ethanol emissions increased considerably between $\lambda = 1$ and $\lambda = 1.24$ and decreased slightly between $\lambda = 1.24$ and $\lambda = 1.34$, the same behavior of the tests with 1500 rpm. The emission of unburnt ethanol was observed to increase steadily with increasing dilution.

Concerning the experiments at 1500 rpm, the variations observed at 2500 rpm differed only in the case of CO_2 and CO. In the case of 1500 rpm, there was a continuous decrease with increasing dilution.

Comparing the emission of gases between the experiments at 1500 rpm and 2500 rpm for the same dilution, it is observed that the CO emission was lower for the condition at 2500 rpm for $\lambda = 1$. For λ greater

than 1.2, the emissions at 2500 rpm were higher. When compared NO_X emissions, it is observed that it was lower for experiments at 2500 rpm. For formaldehyde emissions, as well as THC-ethanol emissions, it was about 5 smaller for 2500 rpm in the condition of $\lambda = 1$ and for the other dilutions, the difference in emissions between the two engine speeds was small. For all dilutions, the emission of unburnt ethanol was lower for the 2500 rpm experiments.

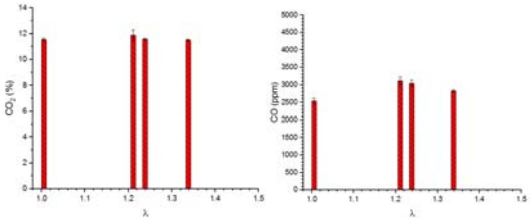

Figure 15. Emissions gas measurement of CO_2 and CO, 2500 rpm, IMEP 1.8 bar.

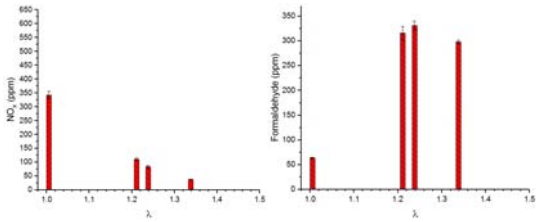

Figure 16. Emissions gas measurement of NO_X and formaldehyde, 2500 rpm, IMEP 1.8 bar.

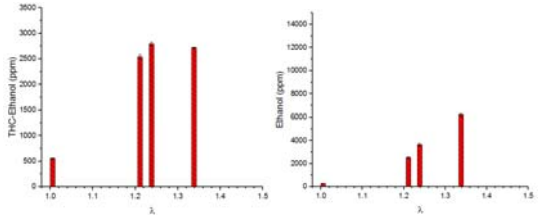

Figure 17. Emissions gas measurement of THC-ethanol and unburned ethanol, 2500 rpm, IMEP 1.8 bar.

CONCLUSION

In the present work, the behavior of air dilution in an internal combustion engine by central direct injection mode using hydrated ethanol with 5% as fuel was analyzed from optical, thermodynamic and emission data. With the increase in dilution, the images showed a gradual increase in the variability of the flame and in its displacement to the region of the inlet valve. This is due to the more characteristic tumble movement in the engine used and to the presence of a greater amount of fuel in that region.

When analyzing the thermodynamic data, it is observed that the same behavior of the images with the linear increase in variability. CovImep values demonstrate this behavior for both engine speeds. Both for 1500 rpm and for 2500 rpm, the 1.5 and 1.4 lambdas, respectively, presented very unstable results. To achieve better results, it is necessary to make modifications to the ignition advance to obtain AI50% results closer to the stoichiometric data. The tests are shown to be important as a preliminary basis to understand the behavior and subsequent comparison with the application of EGR.

ACKNOWLEDGEMENTS

This work was supported by LCPE-ITA and FAPESP-PSA.

REFERENCES

Heywood, J.B., 1988. *Internal Combustion Engine Fundamentals*. McGraw-Hill, Ed.; 1°.; McGraw-Hill: New York, USA.

Desantes, J.M., López, J.J., Molina, S., López-Pintor, D., 2015. "Design of synthetic EGR and simulation study of the effect of simplified formulations on the ignition delay of isooctane and n-heptane". *Energy Convers. Manag*, *96*, 521–531, doi:10.1016/j.enconman.2015.03.003.

Augoye, A., Aleiferis, P., 2015. "Characterization of Flame Development with Hydrous and Anhydrous Ethanol Fuels in a Spark-Ignition Engine with Direct Injection and Port Injection Systems". *SAE Tech. Pap*, *01*, doi:10.4271/2014-01-2623.

Di Iorio, S., Sementa, P., Vaglieco, B., 2015. "Experimental Characterization of an Ethanol DI - Gasoline PFI and Gasoline DI - Gasoline PFI Dual Fuel Small Displacement SI Engine". *SAE Tech. Pap.*, 1–8, doi:https://doi.org/10.4271/2015-01-0848.

Assad, M.S., Kucharchuk, I.G., Penyazkov, O.G., Rusetskii, A.M., Chornyi, A.D., 2011. "Influence of Ethanol on the Operating Parameters of an Internal-Combustion Engine". *J. Eng. Phys. Thermophys*, *84*, 1219–1224.

Varde, K.S.; Manoharan, N.K., 2009. "Characterization of exhaust emissions in a SI engine using E85 and cooled EGR". *SAE Tech. Pap*, *4970*, doi:10.4271/2009-01-1952.

Catapano, F., Sementa, P., Vaglieco, B.M., 2013. "Optical characterization of bio-ethanol injection and combustion in a small DISI engine for two wheels vehicles". *Fuel*, *106*, 651–666, doi:10.1016/j.fuel.2012.11.064.

Abrates, T. T. da S. *Aplicação da técnica PIV em um motor de combustão interna com acesso óptico para estudo dos fenômenos Tumble e Swirl*. [s.l.] Instituto Tecnológico de Aeronáutica, 2017.

Dunn-Rankin, D., Therkelsen, P., 2016. "Lean Combustion Technology and Control". Elsevier, London, UK.

Turns, Stephen R., 2013."Introdução à combustão: Conceitos eaplicações". McGrall Hill AMGH, 3. ed.